Advancing dosimetry for Dating Environmental Materials: Development of an ultra-sensitive beta dosimeter system and potential for beta autoradiography

Martin, L.[1,2,*], Sanderson, D.[1], Paling, S.[3], Cresswell, A.[1], Murphy, S.[1]

[1] Scottish Universities Environmental Research Centre, Glasgow, United Kingdom

[2] Royal Society Newton International Fellow

[3] Boulby Underground Laboratory, Saltburn-by-the-Sea, United Kingdom

[*]Presenting Author: loic.martin@glasgow.ac.uk

Abstract

Beta Dose Rate heterogeneity is a recognized source of uncertainty when applying luminescence dating to heterogeneous samples, such as coarse crystalline rocks and clast-rich sediments. Simulations have shown that a combination of a heterogeneous distribution of minerals and radioactive elements can lead to complex dose distributions, overdispersion and potentially to bias in equivalent dose determinations. However setting realistic conditions for such simulations remains difficult, and there are at present only a few experimental validation cases for such simulated systems. Project ADDEM is investigating means of linking Monte Carlo simulations of dose rate to specific minerals with direct observations using high sensitivity phosphor plates and laser scanning imaging systems in combination with phase mapping. To overcome some of the limitations of autoradiographic imaging of low level beta dose distributions work has been undertaken using Landauer alumina OSL phosphor screens in combination with a laser scanning system developed at the Scottish Universities Environmental Research Centre (SUERC). Preliminary excitation spectra, emission band characterisation and time resolved measurements were undertaken, confirming the potential to recording low doses using asynchronous stimulation at 635 nm coupled with blue band detection. Taking advantage of the slow decay of the luminescence signal the scanning equipment has been configured for pulsed stimulation and asynchronous detection to maximise signal to background ratios. Exploratory work was calibrated using a ^{60}Co facility capable of calibrating doses in the µGy to mGy range. A series of powdered granulite/basalt mixtures of known mean activity and dose rate (Dr) have also been used to calibrate the phosphor screens. To reduce background levels during autoradiographic signal accumulation rock slices are being exposed in the Zeplin shield of the STFC Boulby Underground Laboratory, in an environment which is essentially free from cosmic ray muon background.

Simulations have been conducted providing preliminary deconvolution parameters in order to either reconstruct the beta dose rate (β Dr) distribution received by the grains in the sample, or retrieve the radioactive element distributions in the minerals of the sample, providing the data required for representative simulations of β Dr.

This paper outlines the spectroscopy and sensitivity verification of the autoradiography system, confirming its prospects for measuring spatially resolved β Dr distributions with single pixel lower detection limit of 130 µGy and spatial resolution of 150 µm. Prospects are outlined.

Keywords: beta dose rate; Alumina OSL dosimeter; mapping; simulation; pulsed OSL.

1. Introduction

Beta dose rate (β Dr) heterogeneity in unconsolidated sediments and rocks is a known source of overdispersion in luminescence dating (Nathan et al., 2003). As aliquot sizes have been reduced in response to improved sensitivity in dating analyses it has been highlighted as one of the main sources of overdispersion of equivalent doses, in particular when single grain analyses are involved (Duller et al., 1999). However, β Dr distribution is still difficult to characterize because of the low dose rates of natural samples, the sub-millimetre variations of beta dose rates, and uncertainties associated with in-grain luminescence sensitivity distributions.

Several attempts have been made to map β Dr distributions using phosphor dosimeters (Rufer and Preusser, 2009; Guérin et al., 2012b; Smedley et al., 2020), measurements of β radiation emitting elements (Jankowski and Jacobs, 2018) or semi-conductor detector cluster Timepix (Romanyukha et al., 2017). Despite the new insights that these studies have brought to β Dr heterogeneity, quantification of results remains difficult either because of the lack of a suitable calibration method, of low dosimeter sensitivity leading to large uncertainties, or limitations to spatial resolution on the scale of individual grains and subgrains.

Different approaches aiming to model the beta dose rate distribution instead of measuring it have also been developed. Dose point kernel modelling coupled to 3D phase mapping (Plachy and Sutton, 1982) and Monte Carlo modelling (Nathan et al., 2003; Mayya et al.; 2006, Guérin et al.; 2012a; Martin et al., 2015; Martin et al., 2018) have both shown the capability of modelling beta dose rate distributions of heterogeneous samples. However, the reliability of these methods strongly depends on the exactness of the input data of the model. Therefore they require extensive characterization of samples with a sub-millimetre resolution to be able to resolve the beta dose rate heterogeneity, which in turn is limited by the accuracy and resolution of available methods. In addition, only a few experimental validations of the results of these models for luminescence dating samples have been carried out (Nathan et al., 2003; Cunningham et al., 2012).

The characterization of beta dose rate heterogeneity, in term of intensity and spatial distribution, requires high sensitivity (sub-mGy level), high resolution (sub-mm) and a calibration method adapted to imaging. As a first part of the project ADDEM (Advancing dosimetry for Dating Environmental Materials) we investigated carbon doped alumina (Al_2O_3:C) OSL dosimeter films developed by Landauer Ltd (Glenwood, IL, USA) (Endo et al., 2012) for implementing an ultra-sensitive β autoradiography system suitable for heterogeneous natural samples used in luminescence dating. The properties of this phosphor dosimeter in terms of excitation, decay time and dose response have been investigated for the first part of project ADDEM. These data have been used to improve the signal to noise ratio in a high-resolution laser scanning OSL system. Initial results of Monte Carlo models to calibrate the phosphor response and deconvolve the image to determine the β Dr distribution in the sample are presented.

2. Sample and methodology

2.1 Dosimeter film and samples

Al_2O_3:C is known to be a highly efficient dosimeter for both Optically stimulated Luminescence (OSL) and Thermoluminescence (TL) (McKeever et al., 1999). Although it is well studied in the context of dosimetry for radiation workers, involving Gy level dose or higher (McKeever et al., 1999), fewer studies have considered the sensitivity and dose response curve at mGy and sub-mGy levels (Markey et al., 1995; McKeever and Akselrod, 1999; Kalchgruber et al., 2003). The film used for this study is a 47 µm thick deposit of Al_2O_3:C grains in a polyester binder on a 75 µm thick polyester substrate (Fig. 1). The grains have been measured to be about 15 µm in diameter. The substrate is translucid, allowing luminescence emission in all direction. This film was provided to Scottish Universities Environmental Research Centre (SUERC) as a 22.5 cm by 28 cm sheet that can be cut to the required sizes.

Figure 1

In addition to the high sensitivity of this material a linear dose response curve- is expected from mGy to Gy level. Its linearity for sub-mGy level is investigated during this study. The small thickness of the film will benefit the imaging resolution, as it limits the spreading of beta radiation in the thickness of the sensitive layer, decreasing the need for deconvolution corrections for dose mapping. It is reusable, which combined with the possibility of cutting it to sizes suitable for particular samples makes it practical for regular measurement. The dimensions of the pieces of film cut for this study ranged from 5 mm to 20 mm.

A series of powders of homogenised granulite and of basalt have been prepared at SUERC for use as a new generation of internal dose rate standards (Sanderson personal communication). Here the end members and

mixtures of 50 % and 25 % - 75 % in mass of each have been used, their contents of radioactive elements have been measured by high resolution gamma spectrometry and ICPMS analysis and will be reported elsewhere. Meanwhile table 1 gives the working concentrations of the materials used here. These powders were used for an experiment of exposure of the Al_2O_3:C film to beta dose rate. An inert powder of sodium carbonate Na_2CO_3 was used for blank measurements.

Table 1

2.2 Equipment and method

2.2.1 Excitation spectrometer

Excitation spectra were recorded using the SUERC spectrometer originally developed for research on detection of irradiated foods (Sanderson, 1991), and later applied to studies of feldspars (Clark, 1992; Clark and Sanderson, 1994). Fig. 2 shows a simplified schematic diagram. It uses a 300 W Xenon Cermax lamp as a light source, which incorporates a parabolic reflector resulting in high intensity forward beams. A stepper motor driven Applied Photophysics monochromator, with adjustable slit widths and order sorting filters on entrance and exit for wavelength selection, followed by collimating optics leading to the sample chamber is used. Samples are illuminated on an inclined samples stage. Luminescence is detected using filtered single photon counting tubes (Electron Tubes 9883 QA/QB) with fast amplifier discriminators and recorded using a 2000 channel Ortec multichannel scalar (MCS) system. For this work the PMT was filtered with BG1/BG3 filters to record the near UV and blue emission of the alumina films, with the stimulation light filtered by a 470 nm long pass filter. The luminescence signals from a 5x5 mm piece of Al_2O_3:C film, beta irradiated with 100 Gy, was recorded while the monochromator wavelength was decremented from 750 nm to 480 nm. In earlier work a pyroelectric radiometer was used to normalise the measured spectra (Clark, 1992, Clark and Sanderson, 1994). Here intensity measured were normalized using the theoretical intensity spectra of the Xenon lamp. The excitation spectrum obtained is presented in Fig. 6.

Figure 2

2.2.2 Time resolved OSL reader

Time resolved OSL measurements were made here using diode stimulation, based on pulse generators and transistor driven systems developed in earlier work (Sanderson & Clark, 1994). A schematic of the system used here is shown in (Fig. 3). A TTL oscillator module capable of generating 5 V diode pulses with adjustable pulse widths (down to 1 µs) and delays between pulses ranging from 12 µs to 1.2 s was used. For this study clusters of 3 LEDs of 635 nm wavelength were used to stimulate the sample. The OSL signal is collected by a photomultiplier with a 3 mm BG3 filter. While not completely eliminating the within-pulse background from the 635 nm diodes, this detection band filtration is enough to protect the photomultiplier while allowing more than 80 % of the luminescence signals from the Al_2O_3:C film to pass. While the use of a more efficient wavelength in the 525 nm to 550 nm range would have produced more luminescence per unit of time, this would have been too close to the main emission band of Al_2O_3:C and therefore requiring a larger thickness of BG3 filter (12 mm minimum) in order to protect the photomultiplier. This would significantly decrease the luminescence signal passing through the filter, at the point that the signal measured is not significantly more than with the 635 nm stimulation and 3 mm BG3 filter. In addition, for the laser scanning system that is described below, the use of 525 nm to 550 nm wavelength laser increases the risk of damaging the photomultiplier in case of a direct beam reflection. It also prevents the possibility of doing successive imagings of the same irradiation, as the bleaching of luminescence signal by the laser would also be significantly faster than with the 635 nm laser stimulation.

The detection during a defined time window was synchronised by starting MCS capture at the beginning of each stimulation pulse using the TTL drive signal. The counts from each stimulation pulse were then registered in the MCS and used to define the luminescence relaxation decay times. Similar systems were used by Markey et al. (1995) or Yukihara and McKeever (2006) to perform time resolved analysis of Al_2O_3:C. The time resolved

analysis of a 5x5 mm piece of Al_2O_3:C film irradiated with 100 Gy is presented on Fig.7, recorded using 130ms stimulation pulses with a 1500 ms delay, over about 20 min.

Figure 3

2.2.3 Laser scanning imaging OSL reader

The imaging OSL readers from Sanderson et al. (2001) (Fig. 4) were designed to map the luminescence signal from a sample pixel by pixel. The sample is placed on a support on a plate moved by two perpendicular stepper motor axes (X and Y axis). Based on the review of the excitation and time resolved spectrometry of the alumina film one of these systems has been configured with a 635 nm 5 mW Acculase model laser from Global Laser LTD (Abertillery, UK), and detection band photon counting with BG3 filtration. The laser has a beam size at nearest focus of < 50 µm, bringing the beam from a working distance of 10 cm at a 45° angle results in a spot size <100 µm at this stage of the work. The luminescence is recorded by a photomultiplier above the sample, then the plate moves one step for the next measurement. Setting the system up in this way allows the luminescence signal measured from the sample during the decay after stimulation to be optimised while using a pulsed OSL (pOSL) protocol (Markey et al.,1995; McKeever and Akselrod, 1999, Yukihara and McKeever, 2006). The stimulation sequence is composed of successive stimulation pulses followed by measurements of the luminescence signal during its decay. This protocol was chosen in consideration of the properties of the OSL film determined by the previous analysis (see Results part). The measurements on each point are preceded by several dark count measurements. This succession of dark count measurement is used to determine if a luminescence or phosphorescence signal persists from the previous measurement, by comparison of dark count prior to the start of any measurement and by checking if the signal is decaying. No significant signal remaining from the previous point of measurement was observed in this study. The average dark count was calculated as the mean value over successive measurements.

Figure 4

2.2.4 Irradiation of dosimeter films

In order to estimate the signal from sub-mGy doses and to test the linearity of the film response to dose, a piece of 10x15 mm film was irradiated using a ^{60}Co gamma source with doses from 139 ± 8 to 739 ± 33 mGy. The piece of film was covered a 3 mm of aluminium sheet during gamma irradiation in order to generate charge particle equilibrium. Before each irradiation, the sample was bleached under white light, through a GG 495 nm long pass filter to cut UV wavelength and reduce charge transfer from deep traps during bleaching. It was then scanned with the laser scanning OSL reader using 500 µm steps and a sequence of 300 ms of dark count measurement followed by 100 repetitions of the cycle “60 ms of laser stimulation – 30 ms of measurement during the luminescence signal decay”. The resulting images can be observed in Fig. 8, while the calibration curve resulting from the integrated signals over the image is presented in Fig. 9. Limits of detection and of quantification resulting from these results are illustrated in Fig. 10 .

2x2 cm pieces of dosimeter film were exposed to powdered samples of granulite-basalt mixtures (table 1) and pure sodium carbonate, the last one being used as blank. They were bagged in pairs in dark polyethylene 75 µm thick bags, which is enough to shield from the alpha particles and protect the phosphor from light exposure, with the sensitive parts turned outwards. The bagged dosimeter films were placed in the centre of 5 cm diameter by 1.8 cm high cylindrical plastic containers filled by the powder samples, according to the geometry presented in Fig. 5a. This ensures that the bagged films are surrounded by at least 5 mm of powder on every side, which is enough to create an infinite matrix condition in regard of the beta dose rate. The containers were placed in a 10 cm thick lead castle with a 1.5 mm inner layer of copper (Fig. 5b), for shielding from the environmental X-rays and gamma radiation, as well as from the soft cosmic component. The exposure time was about 1 year and 4 months. The dose rates were estimated using the radioactive element contents from table 1, and the conversion factors from Cresswell et al. (2018). The beta attenuation factors by the dosimeter and protective layer were calculated

from modelling, as well as the gamma dose rate contribution (table 2). Each calculated dose was adjusted considering the exact time of exposure within an uncertainty of one day. They were read with the laser scanning OSL reader using 250 µm steps and a sequence of 300 ms of dark count measurement followed by 100 repetitions of the cycle "60 ms of laser stimulation – 30 ms of measurement during the luminescence signal decay". They were then bleached for 48 h under non-UV white light and scanned again to measure the background signal. The results of counts per pixel compared to the estimated dose are plotted on Fig. 11a. Equivalent gamma dose for the measured luminescence signal were obtained by irradiating the same dosimeter film with a calibrated ^{60}Co gamma source: each film was exposed to a dose of 900 µGy and their luminescence signal was measured again using the same protocol; the ratios of powder exposure signal to the gamma source exposure signal were used to calculate the gamma doses equivalent to the powder exposure signal. These equivalent doses are compared with the calculated exposure dose on Fig. 11b.

2.3 Modelling

Monte Carlo simulations of the irradiation of the film were conducted to calculate the attenuation during exposure of the sample and to investigate the correspondence between the mapped OSL signals and the Dr distribution in the sample. There were conducted using the Geant4 toolkit (Agostinelli et al., 2003; Allison et al., 2016), that already have been successfully used in the context of luminescence dating (Guérin et al.; 2012a; Martin et al., 2015; Martin et al., 2018). The simulation code allows stacking different types of slices: radioactive mineral, phosphor, phosphor substrate, phosphor cover, absorber. The composition and density of each type can be adjusted. The phosphor layer is divided into pixels of adjustable size, each pixel records the dose received from the radioactive mineral layer. The distribution of radioactivity in this layer can be uniform or follow certain patterns such as a rectangle, a dot or a sphere. The spectra for the beta and gamma emissions of ^{40}K, of U-series and of Th-series were constructed using the Geant4 database, whose data comes from the Evaluated Nuclear Structure Data File (ENSDF) which is maintained by the National Nuclear Data Center, Brookhaven National Laboratory (USA). It is noted that emission spectra in other nuclear databases vary from the ENSDF used here, as recently discussed by Cresswell et al. (2019), but these differences have not currently been considered. The PENELOPE code for low-energy particle physics (Baró et al., 1995; Ivanchenko et al., 2011) was used for calculating the beta interactions through matter.

Simulations of the exposure of two OSL films protected by a 75 µm thick dark plastic bag to granulite powder (composition given in table 1, density 2.0 g.cm^{-3}) were conducted (Fig. 5a). The resulting beta attenuation coefficients are presented in Table 2. The gamma dose contribution to the exposure dose of the films was simulated from each position of the powder container, in order to investigate both the contribution from the powder in the same container as the film and the contribution from powder in the other containers (Fig. 5b). The backscattering effect was taken into account by reproducing the lead and copper shielding where the containers were placed during the film exposure.

In order to investigate the difference of the Dr distribution in the samples and the Dr distribution received by the phosphor film, two simulations of a virtual sample made of a K-feldspar half-part irradiating an inert quartz half using the ^{40}K beta spectrum were set up: the first with a quartz layer of negligible thickness (1 µm) between two 5mm thick slices of samples (Fig. 5c) in order to determine the natural spreading of Dr in it, the second represents an OSL film protected by an alpha-thick dark low-density polyethylene (PDTE) bag and placed between two 5 mm thick slices of samples (Fig. 5d) in order to observe the Dr spreading resulting from the exposure to beta emissions. The results are compared on Fig. 12.

Figure 5

3. Results

Figure 6

The sensitivity to excitation of the OSL film increases from the 750 nm wavelength, where it is almost negligible, to the 475 nm (Fig. 6). This is in agreement with previous measurements of the Al_2O_3:C excitation spectrum by Chruścińska (2016). Although it seems more efficient to stimulate this phosphor in lower wavelengths around 500 nm, it would be too close to the Al_2O_3:C main emission peaks around 330 nm and 425 nm (Yukihara and McKeever, 2006). This would lead to either significant risk of damaging the photomultiplier or using thick of optical filters reducing the luminescence signal measured.

Figure 7

The time resolved OSL analysis of the phosphor indicates two slowly decaying components of the luminescence signal, with time constants of 24.0 ± 0.1 ms and 248 ± 13 ms respectively (Fig. 7). These two components where previously measured by Summer (1984) as well as by Markey et al. (1995) to approximatively 35 ms, corresponding to the F-center lifetime, and to approximatively 545 ms at 25°C, this second component being temperature dependant according to measurements from room temperature to 100 °C from Markey et al. (1995). Though of the same order of magnitude, the decay constants measured in this study at ambient temperature are significantly shorter than those measured by Markey et al. (1995). The reason for this difference is not clear but will be investigated in further studies.

Figure 8

Maps of the luminescence signals from the gamma irradiations (Fig. 8) indicate a homogeneous signal in this piece of film, with some statistical variations. A significant background signal can be seen on the blank image; this background cannot be bleached either using white light or the laser stimulation.

The luminescence signal corresponding to the edge of the film is lower than the signal in the central part, probably resulting from the laser beam stimulating an area overlapping the sample and the support filter For this reason, when integrating the signals from multiple pixels, the outermost 2 pixels (corresponding to an area up to 1 mm away from the edge) were not taken into account. The calibration curve resulting from these integrations indicates a linear response of this OSL film to dose (Fig. 9), as was previously observed by Markey et al. (1995). The 2σ uncertainties indicated on the abscise axis results from the quadratic sum of the relative uncertainties on the gamma source calibration and on the exposure time. The uncertainties on the signal counts were calculated as the quadratic sum of the absolute values of the uncertainties on the dark count, on the background counts and on the luminescence counts (whose standard deviation was estimated as the square root of the counts), all integrated over an area of approximatively 35 mm^2. The final uncertainties remain under 2 % at 2σ and therefore cannot be seen on Fig. 9.

Figure 9

The dark count integrated over the same area as the OSL signal ranged from 87 to 124 counts per point of measurement (corresponding to a 3 s measurement), with a maximum standard deviation of 18 counts. The average background signal was measured on the blank to 123 counts per point of measurement, with a standard deviation of 10 counts after quadratic subtraction of the dark count standard deviation during this analysis. The limits of detection L_{det} and the limits of quantification L_{qt} are calculated for different surface of integration on Fig. 10. The formula used for calculating these values are:

$$L_{det} = 3(\Delta_{DC}^2 + \Delta_{BG}^2)^{0.5}.(N-1)^{-0.5} \quad (1)$$

$$L_{qt} = 10(\Delta_{DC}^2 + \Delta_{BG}^2)^{0.5}.(N-1)^{-0.5} \quad (2)$$

Where Δ_{DC} is the maximum standard deviation of the dark count, Δ_{BG} is the standard deviation of the background measurement, and N is the number of measured points that were integrated. The measurements presented on Fig. 9 were integrated over an area of about 560 measurement points, resulting in a L_{det} of 5 µGy and a L_{qt} of 18 µGy.

Figure 10

Table 2

The simulations calculated a significant attenuation of the beta dose rate, resulting from the shielding by the protective layer and by the substrate of the Al_2O_3:C as well as from the missing radiation from the volume occupied by the dosimeters and plastic bags (Table 2). This attenuation is different for the different beta spectra. An average value of attenuation factor can be calculated to 0.66 ± 0.01 considering the proportion of radioactive elements in the granulite powder or to 0.65 ± 0.01 considering the proportion of radioactive elements in the basalt powder or in a typical sediment (Aitken, 1985). The gamma dose contribution represents 7 % to 8 % of the total exposure dose, with 87 % to 58 % of the gamma dose (for the granulite powder and the basalt powder respectively) coming from the same container as the film, the rest of the gamma dose contribution coming from the other containers.

Figure 11

Fig. 11a seems to indicate a linear response to dose of the pieces of film exposed to the powder samples. The lower slope than for the gamma irradiated film results (Fig. 9) may indicates a variability in signal to dose response of the film. The intercept (with a value of 94 ± 31 cps) indicates the environmental dose received by the sample during the time of exposure, corresponding to 304 ± 99 µGy, equivalent to a dose rate of 0.23 ± 0.08 mGy.y^{-1}. This is compatible with the hard cosmic radiation component at sea level. Fig. 11b shows a good consistency between the calculated exposure doses and the equivalent gamma doses, with a ratio of 1.02 ± 0.07 determined by the slope value.

Figure 12

The dose profile obtained from simulation of exposure highlight a difference of spatial distribution between the dose in the sample and the dose received by the phosphor (Fig. 12). This difference is due to the non-negligible thickness of the detector and its cover compared to the average beta range: it represents an inert layer of 272 µm where the beta particles from the sample spread, that will result in an effect comparable to a blurring on the image obtained by laser scan of the dosimeter. Because of this, the beta dose rate image should require a deconvolution or another method in order to take in account the decreasing of apparent variation of the dose rate due to the blurring effect.

4. Discussion

This Al_2O_3:C OSL film is sensitive enough to detect sub-mGy doses, with a linear dose response from µGy to mGy levels (Fig. 9 and fig. 11). The significant background signal may limit the accuracy for low dose mapping. Further studies will investigate the possibility of bleaching this background signal using temperature or different stimulation wavelengths. Unfortunately, the polyester nature of the substrate and the binder limit the temperature to the which the film can be exposed.

When comparing the OSL signals from the gamma irradiated film (Fig. 9) and the film pieces exposed to the powder samples (Fig. 11a), it appears that the second is about 30% lower for the same dose. Several hypotheses are currently under investigation in order to explain this difference in response. The most likely is that the sample support used for the films exposed to powder was different than the support used for the gamma irradiated piece of film, what put the firsts 3 mm further from the photomultiplier than the second, resulting in a smaller solid angle for the luminescence photon to reach the detector. The comparison between the calculated exposure doses and the equivalent gamma dose shows a good correlation (Fig. 11b), which validates the beta and gamma contributions calculated by simulations (Table 2) and indicates that the sensitivity of the film to gamma exposure is similar to beta exposure.

The sub-mGy L_{qt} (422 µGy per measurement point) enables the possibility of a pixel-by-pixel calibration of the measurement for long enough exposure time, leading to high resolution mapping of Dr. This L_{qt} can be brought under 100 mGy by integrating areas of about 20 pixels, in order to limit the time of exposure to sample to a few weeks. This corresponds to areas of 5 mm^2 for 500 µm pixels (equivalent to a resolution of 2.24 mm) or 0.45 mm^2 for 150 µm pixels (equivalent to a resolution of 0.67 mm). A strategy to benefit from this would be to identify the homogeneous areas and to integrate the signal over these, in order to lower the L_{qt} and to increase the accuracy

of the Dr measurement for these areas. However this may not be always possible in the case of heterogeneous sample exposure. It is always possible to obtain higher resolutions and accuracy by longer exposure time, or with sample with a higher radioactivity such as granite and granulite.

The environmental background Dr during exposure is another parameter that can limit the accuracy of the measurement. Fig. 11 shows that it is necessary to set up a blank in order to measure this environmental Dr contribution, but it is better to shield against environmental radiation as much as possible to preserve the accuracy of the measurement. Samples under exposure can be placed in containers thick enough to shield them from beta radiation from other samples. The use of a lead shield can efficiently cut the gamma radiation and the soft component of cosmic radiation, while X-rays from atomic deexcitation and from Bremsstrahlung radiation can be efficiently shielded using inert copper. Using such shielding, we can see on fig. 11 that the environmental background can be reduced to about 0.23 ± 0.08 mGy.y^{-1}, which is the order of magnitude of the hard component of cosmic radiations at sea level. Unfortunately, this is still enough to produce OSL signal of the same order of magnitude as the dark count of the photomultiplier or as the observed background signal of the Al_2O_3:C film. This would lead to higher limit of detection and quantification, significantly reducing the accuracy of sub-mGy level measurements.

The reduction of the highly penetrating cosmic radiation component is more problematic as it needs several meters of rock to be significantly attenuated. In order to benefit from an environment extremely clean from cosmic radiation, OSL film exposures to granulite slices are currently underway in the STFC Boulby Underground Laboratory (Saltburn-by-the-Sea, UK). This laboratory is built 1.1 km underground, efficiently reducing the cosmic radiation Dr to a negligible level with a muon reduction factor of 10^6 (Murphy and Paling, 2012). Each sample and film were placed in pure quartz containers of 1 mm thickness, so each is separated from surrounding samples by 2 mm of quartz which is enough to absorb more than 99% of the natural beta radiation. The samples are shielded from X-rays and gamma radiation by pure copper bricks of 5 cm to 10 cm thickness (Fig. 13a) and by a 20cm thick Zeplin lead shield (Fig. 13b).

Figure 13

The simulation results from Fig. 12 point out a major issue of the beta dose rate imaging: the dose distribution on the image can be different from the dose distribution in the sample, depending on the detector characteristics and geometry. This may indicate that the quantification of beta dose rate distribution from previous studies that did not consider this effect may be biased (Romanyukha et al. 2017; Smedley et al., 2020); in particular the beta dose rate dispersion could be underestimated. It is noticeable that even if the distribution of the dose received in the phosphor is different than in the sample, the calibrated dose value resulting from the integration over the whole sensitive area (with the exclusion of the edge potentially affected by edge effect) should be the same (equal to half of the infinite matrix dose of the radioactive part in the case of this modelling). The only difference is the higher spreading of the beta in the detector, resulting in what could be described as a "blurring effect" in the imaging of the dose distribution. Simulations adapted to the geometry of sample exposure could be used to calculate deconvolution parameters, such as point spread functions, in order to deconvolve the dose image for reconstructing the dose distribution in the sample.

5. Conclusion

This study demonstrates the high potential of Landauer's Al_2O_3:C OSL dosimeter films for imaging the beta dose rate, in combination with the developed protocol of laser scanning pulsed OSL and with Monte Carlo simulation for calculating attenuation factors and eventual deconvolution parameters. It presents a linear dose response from µGy to mGy level, and a limit of quantification per point in the sub-mGy level. Quantification below 100 µGy can be achieved by integrating over a few pixels. This is enough to obtain an accurate Dr image of natural samples over a few weeks to a few months of exposure time, especially if benefiting from a very low environmental background such as is reachable in underground laboratories. A high resolution of 150 µm can be achieved using

the described laser scanning OSL reader, but the necessity to integrate the signal over several pixels in order to reach an acceptable accuracy may reduce this resolution for low dose exposure.

Experiments are currently under way in order to test the imaging of beta dose rate of heterogeneous samples. It will benefit from the ultra-low environmental background reachable at the STFC Boulby Underground Laboratory, and of image deconvolution processing with parameters obtained from the beta simulation results. Future work will also apply the techniques described here to rock samples.

Acknowledgements

This research has been funded by the Royal Society through a Newton International Fellowship. The authors are thankful to Frances Pearce from Landauer for providing the dosimeter sheet.

References

Agostinelli, S., Allison, J., Amako, K., Apostolakis, J., Araujo, H., Arce, P., Asai, M., Axen, D., Banerjee, S., Barrand, G., Behner, F., Bellagamba, L., Boudreau, J., Broglia, L., Brunengo, A., Burkhardt, H., Chauvie, S., Chuma, J., Chytracek, R., Cooperman, G., Cosmo, G., Degtyarenko, P., Dell'Acqua, A., Depaola, G., Dietrich, D., Enami, R., Feliciello, A., Ferguson, C., Fesefeldt, H., Folger, G., Foppiano, F., Forti, A., Garelli, S., Giani, S., Giannitrapani, R., Gibin, D., Cadenas, J.J. Gomez, Gonzlez, I., Abril, G. Gracia, Greeniaus, G., Greiner, W., Grichine, V., Grossheim, A., Guatelli, S., Gumplinger, P., Hamatsu, R., Hashimoto, K., Hasui, H., Heikkinen, A., Howard, A., Ivanchenko, V., Johnson, A., Jones, F.W., Kallenbach, J., Kanaya, N., Kawabata, M., Kawabata, Y., Kawaguti, M., Kelner, S., Kent, P., Kimura, A., Kodama, T., Kokoulin, R., Kossov, M., Kurashige, H., Lamanna, E., Lampen, T., Lara, V., Lefebure, V., Lei, F., Liendl, M., Lockman, W., Longo, F., Magni, S., Maire, M., Medernach, E., Minamimoto, K., de Freitas, P. Mora, Morita, Y., Murakami, K., Nagamatu, M., Nartallo, R., Nieminen, P., Nishimura, T., Ohtsubo, K., Okamura, M., O'Neale, S., Oohata, Y., Paech, K., Perl, J., Pfeiffer, A., Pia, M.G., Ranjard, F., Rybin, A., Sadilov, S., Salvo, E. Di, Santin, G., Sasaki, T., Savvas, N., Sawada, Y., Scherer, S., Sei, S., Sirotenko, V., Smith, D., Starkov, N., Stoecker, H., Sulkimo, J., Takahata, M., Tanaka, S., Tcherniaev, E., Tehrani, E. Safai, Tropeano, M., Truscott, P., Uno, H., Urban, L., Urban, P., Verderi, M., Walkden, A., Wander, W., Weber, H., Wellisch, J.P., Wenaus, T., Williams,D.C., Wright, D., Yamada, T., Yoshida, H., Zschiesche, D., , 2003. Geant4–a simulation toolkit. Nuclear Instruments and Methods in Physics Research Section A: Accelerators, Spectrometers, Detectors and Associated Equipment, 506(3), 250-303.

Aitken, M.J., 1985. Thermoluminescence Dating. Academic Press, London, 378 p.

Allison, J., Amako, K., Apostolakis, J., Arce, P., Asai, M., Aso, T., Bagli, E., Bagulya, A., Banerjee, S., Barrand, G., Beck, B.R., Bogdanov, A.G., Brandt, D., Brown, J.M.C., Burkhardt, H., Canal, Ph., Cano-Ott, D., Chauvie, S., Cho, K., Cirrone, G.A.P., Cooperman, G., Cortés-Giraldo, M.A., Cosmo, G., Cuttone, G., Depaola, G., Desorgher, L., Dong, X., Dotti, A., Elvira, V.D., Folger, G., Francis, Z., Galoyan, A., Garnier, L., Gayer, M., Genser, K.L., Grichine, V.M., Guatelli, S., Guèye, P., Gumplinger, P., Howard, A.S., Hřivnáčová, I., Hwang, S., Incerti, S., Ivanchenko, A., Ivanchenko, V.N. , Jones, F.W., Jun, S.Y., Kaitaniemi, P., Karakatsanis, N., Karamitros, M., Kelsey, M., Kimura, A., Koi, T., Kurashige, H., Lechner, A., Lee, S.B., Longo, F., Maire, M., Mancusi, D., Mantero, A., Mendoza, E., Morgan, B., Murakami, K., Nikitina, T., Pandola, L., Paprocki, P., Perl, J., Petrović, I., Pia, M.G., Pokorski, W., Quesada, J.M., Raine, M., Reis, M.A., Ribon, A., Ristić Fira, A., Romano, F., Russo, G., Santin, G., Sasaki, T., Sawkey, D., Shin, J.I., Strakovsky, I.I., Taborda, A., Tanaka, S., Tomé, B., Toshito, T., Tran, H.N., Truscott, P.R., Urban, L., Uzhinsky, V., Verbeke, J.M., Verderi, M., Wendt, B.L., Wenzel, H., Wright, D.H., Wright, D.M., Yamashita, T., Yarba, J., Yoshida, H., 2016. Recent developments in GEANT4. Nuclear Instruments and Methods in Physics Research A 835, 186–225.

Baró, J., Sempau, J., Fernández-Varea, J.M., Salvat, M., 1995. “PENELOPE”: an algorithm for Monte Carlo simulation of the penetration and energy loss of electrons and positrons in matter. Nuclear Instruments Methods in Physics Research B 100 : 31-46.

Chruścińska, A., 2016. Optical depth of traps in AL2O3:C determined by the variable energy of stimulation OSL (VES-OSL) method. Radiation Measurements 90, pp. 94-98. DOI: 10.1016/j.radmeas.2016.01.032.

Clark R.J., 1992, Photostimulated Luminescence as an Archaeological dating tool, PhD thesis, University of Glasgow, https://theses.gla.ac.uk/74653/

Clark, R.J., Sanderson, D.C.W., 1994. Photostimulated luminescence excitation spectroscopy of feldspars and mica. Radiation Measurements 23, 641-646.

Cresswell, A.J., Carter, J., Sanderson, D.C.W., 2018. Dose rate conversion parameters: Assessment of nuclear data. Radiation Measurements 120, pp. 195-201. DOI: 10.1016/j.radmeas.2018.02.007

Cresswell, A.J., Sanderson, D.C.W. & Carter, J., 2019. Review of nuclear data for naturally occurring radionuclides applied to environmental applications. Eur. Phys. J. Plus 134, 69. https://doi.org/10.1140/epjp/i2019-12437-1

Cunningham, A.C., DeVries, D.J., Schaart, D.R., 2012. Experiment and computational simulation of beta-dose heterogeneity in sediment. Radiation Measurements 47, 1060-1067

Duller, G.A.T., Bøtter-Jensen, L., Murray, A.S., Truscott, A.J., 1999. Single grain laser luminescence (SGLL) measurements using a novel automated reader. Nuclear Instruments and Methods B 155, 506-514.

Endo, A., Katoh, T., Kobayashi, I., Joshi, R., Sur, J., Okano, T., 2012. Characterization of optically stimulated luminescence dosemeters to measure organ doses in diagnostic radiology, Dentomaxillofac Radiol. 41-3, pp. 211–216.

Guérin, G., Mercier, N., Nathan, R. , Adamiec, G. and Lefrais, Y., 2012a. On the use of the infinite matrix assumption and associated concepts: a critical review. Radiation Measurements 47, 778 – 785.

Guérin, G., Discamps, E., Lahaye, C., Mercier, N., Guibert, P., Turq, A., Dibble, H.L., McPherron, S.P., Sandgathe, D., Goldberg, P., Jain, M., Thomsen, K., Patou-Mathis, M., Castel, J.-C., Soulier, M.-C., 2012b. Multi-method (TL and OSL), multi-material (quartz and flint) dating of the Mousterian site of Roc de Marsal (Dordogne, France): correlating Neanderthal occupations with the climatic variability of MIS 5–3. Journal of Archaeological Science 39, 3071-3084.

Ivanchenko, V., Apostolakis, J., Bagulya, A., Abdelouahed, H.B., Black, R., Bogdanov, A., Burkhard, H., Chauvie, S., Cirrone, P., Cuttone, G., Depaola, G., Di Rosa, F., Elles, S., Francis, Z., Grichine, V., Gumplinger, P., Gueye, P., Incerti, S., Ivanchenko, A., Jacquemier, J., Lechner, A., Longo, F., Kadr, O., Karakatsanis, N., Karamitros, M., Kokoulin, R., Kurashige, H., Maire, M., Mantero, A., Mascialino, B., Moscicki, J., Pandola, L., Perl, J., Petrovic, I., Ristic-Fira, A., Romano, F., Russo, G., Santin, G., Schaelicke, A., Toshito, T., Tran, H., Urban, L., Yamashit, T., Zacharatou, C., 2011. Recent improvements in Geant4 electromagnetic physics models and interfaces. Progress in Nuclear Science and Technology 2, 898-903.

Jankowski, N. R., Jacobs, Z., 2018. Beta dose variability and its spatial contextualisation in samples used for optical dating: An empirical approach to examining beta microdosimetry. Quaternary Geochronology, 44, pp. 23-37.

Kalchgruber, R., Fuchs, M., Murray, A. S., & Wagner, G. A., 2003. Evaluating dose-rate distributions in natural sediments using α-Al2O3: C grains. Radiation Measurements, 37(4-5), 293-297.

Mayya, Y.S., Morthekai, P., Murari, M.K., Singhvi, A.K., 2006. Towards quantifying beta microdosimetric effects in single-grain quartz dose distribution. Radiation Measurements 41, 1032-1039.

Martin, L., Mercier, N., Incerti, S., Lefrais, Y., Pecheyran, C., Guerin, G., Jarry, M., Bruxelles, L., Bon, F., Pallier C., 2015. Dosimetric study of sediments at the Beta dose rate scale : characterization and modelization with the DosiVox software. Radiation Measurement 81, 134-141

Martin L., Fang F., Mercier N., Incerti S., Grün R., Lefrais Y., 2018. 2D modelling: A Monte Carlo approach for assessing heterogeneous β Drs in luminescence and ESR dating: Paper I, theory and verification. Quaternary Geochronology 48, pp. 25-37

McKeever, S.W.S., Akselrod, M.S., 1999. Radiation dosimetry using pulsed optically stimulated luminescence of Al_2O_3:C. Radiation Protection Dosimetry 84, pp. 317–320.

McKeever, S.W.S., Akselrod, M.S., Colyott, L.E., Agersnap Larsen, N., Polf, J.C., Whitley, V. (INVITED), 1999. Characterisation of Al2O3 for Use in Thermally and Optically Stimulated Luminescence Dosimetry, Radiation Protection Dosimetry, Volume 84, Issue 1-4, pp. 163–166, https://doi.org/10.1093/oxfordjournals.rpd.a032709

Markey B. G., Colyott L. E. and McKeever S. W. S., 1995. Time-resolved optically stimulated luminescence from Al_2O_3:C. Radiation Measurements 24, pp. 457-46

Murphy, A. and Paling, S., 2012. The Boulby Mine Underground Science Facility: The Search for Dark Matter, and Beyond. Nuclear Physics News 22:1, pp. 19-24. DOI: 10.1080/10619127.2011.629920

Nathan, R.P., Thomas, P.J., Jain, M., Murray, A.S., Rhodes, E.J., 2003. Environmental dose rate heterogeneity of beta radiation and its implications for luminescence dating: Monte Carlo modelling and experimental validation. Radiation Measurement 37, 305-313.

Plachy, A. L., Sutton,S. R., 1982. Determination of the Dose-rate to Quartz in Granite. PACT 6, pp.188-194.

Romanyukha, A. A., Cunningham, A. C., George, S. P., Guatelli, S., Petasecca, M., Rosenfeld, A. B., Roberts, R. G., 2017. Deriving spatially resolved beta dose rates in sediment using the Timepix pixelated detector. Radiation Measurements 106, pp. 483-490. DOI: 10.1016/J.RADMEAS.2017.04.007

Rufer, D., Preusser, F., 2009. Potential of autoradiography to detect spatially resolved radiation patterns in the context of trapped charge dating. Geochronometria 34, 1-13.

Sanderson, D.C.W., 1991. Photostimulated luminescence (PSL): A new approach to identifying irradiated foods, EUR 13331 report, pp. 159-167

Sanderson, D.C.W., Clark, R.J., 1994. Pulsed photostimulated luminescence of alkali feldspars. Radiation Measurements 23, 633-639

Sanderson D.C.W.,Carmichael L.A., Murphy S., Whitely V., Scott E.M., Cresswell A., 2001. Statistical and Imaging Methods for luminescence detecvtion of irradiated Ingredients, Food Standards Agency, London, Project CSA 5240. Available from http://eprints.gla.ac.uk/58359

Smedley, R. K., Duller, G. A. T., Rufer, D., & Utley, J. E. P., 2020. Empirical assessment of beta dose heterogeneity in sediments: Implications for luminescence dating. Quaternary Geochronology, 56, [101052]. https://doi.org/10.1016/j.quageo.2020.101052

Summers, G. P., 1984. Thermoluminescence in single crystal α-Al2O3. Radiation Protection Dosimetry 8, 69-80

Yukihara, E. G. and McKeever, S. W. S., 2006. Spectroscopy and optically stimulated luminescence of Al_2O_3:C using time-resolved measurements. Journal of Applied Physics 100, issue 8; https://doi.org/10.1063/1.2357344

Figure 1 (1.5 column): Geometry and composition of the Landauer Al_2O_3:C OSL film

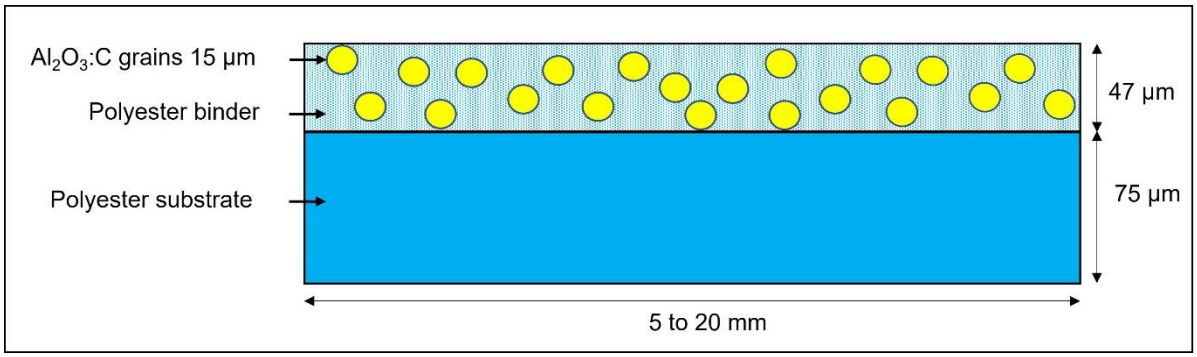

Figure 2 (single column): excitation spectrometer schematic

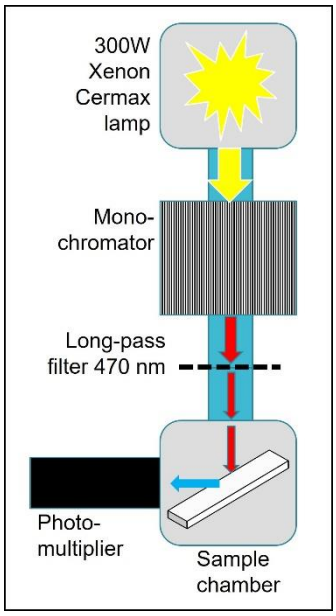

Figure 3 (single column): Time resolved OSL reader schematic

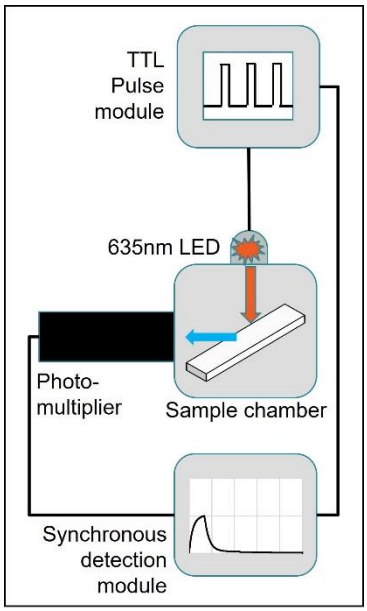

Figure 4 (single column): Laser scanning imaging OSL reader schematic

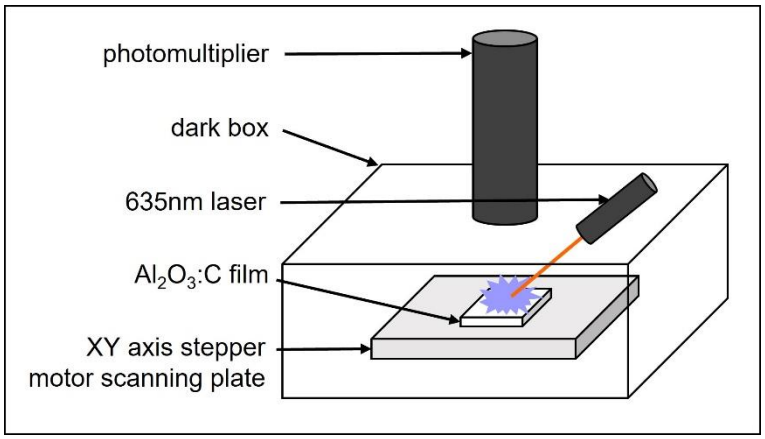

Figure 5 (single column): Geometries of the Geant4 simulations

a – Dosimeter exposure to powdered sample

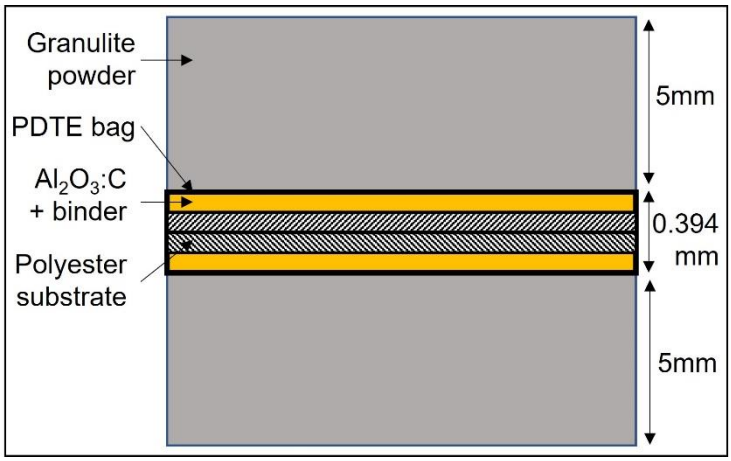

b – Sample containers in the environmental radiation shield

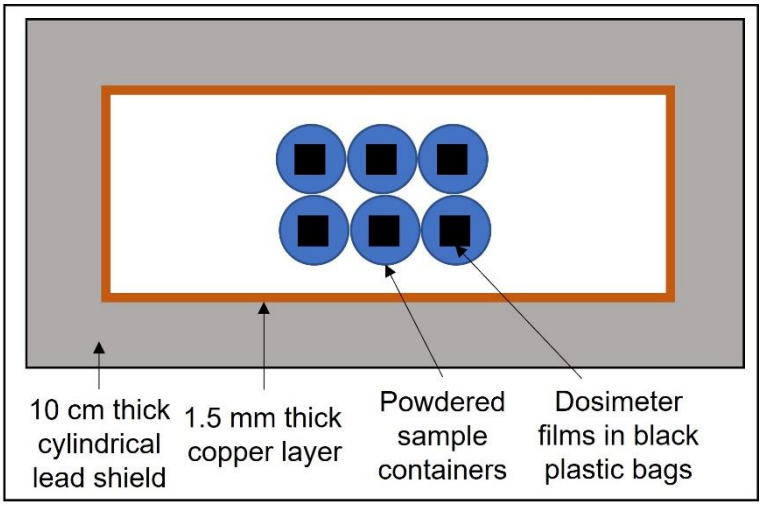

c –Dose rate distribution in a K-feldspar-Quartz sample

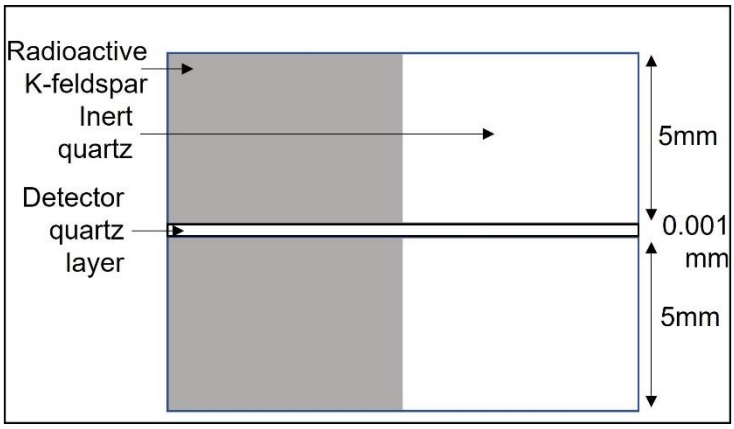

d – Dosimeter exposure to a K-feldspar-Quartz sample

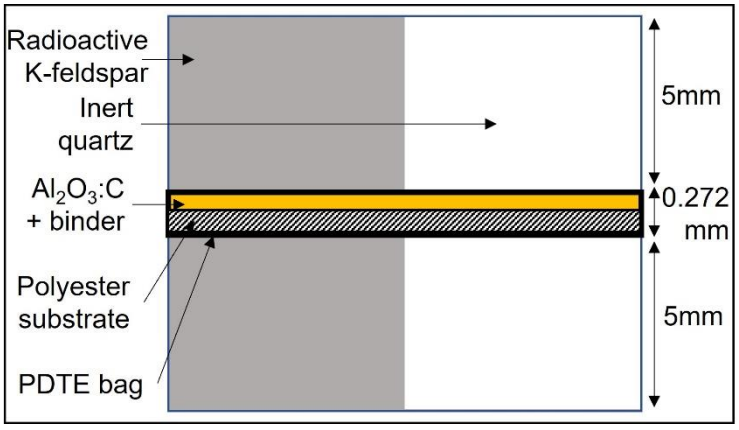
Radioactive
K-feldspar
Inert
quartz
Al_2O_3:C
+ binder
Polyester
substrate
PDTE bag
5mm
0.272
mm
5mm

Figure 6 (single column): Excitation spectrum of the Al_2O_3:C film

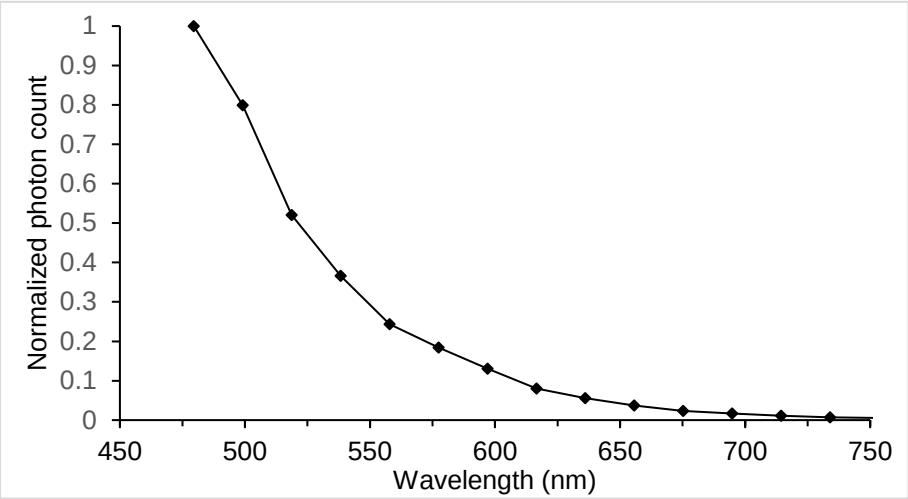

Figure 7 (single column): Pulse stimulated OSL of the Al_2O_3:C film. *The pulse duration is 130ms and the delay between pulses is 1500ms. The signal decay after the pulse is best fitted by a double exponential decay with half-time constants of 24.0 ± 0.1 ms and 248 ± 13 ms*

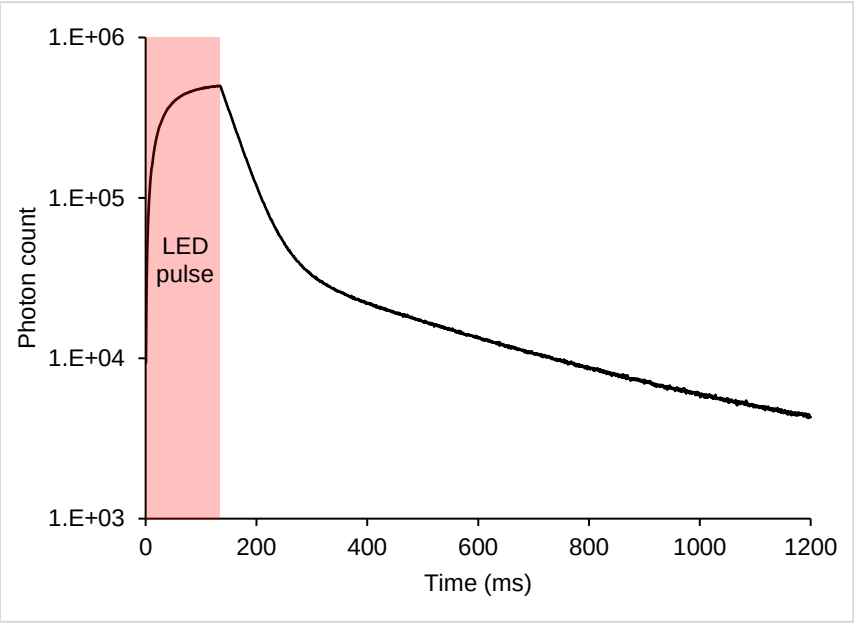

Figure 8 (2 columns): OSL imaging of a piece of Al_2O_3:C film. *The dark counts were not subtracted. The background from the sample support can be observed around the piece of film and is not significantly higher than the dark counts value, indicating that there is no significant scattering of the laser beam nor luminescence from the support. A high-count pixel can be seen out of the film area, near the top right corner of the 295 µGy image. Its origin is under investigation and they are removed from analysis when occurring in the film area. It can be seen that the piece of film lightly shifted between scanning, due to the support that have been improved since.*

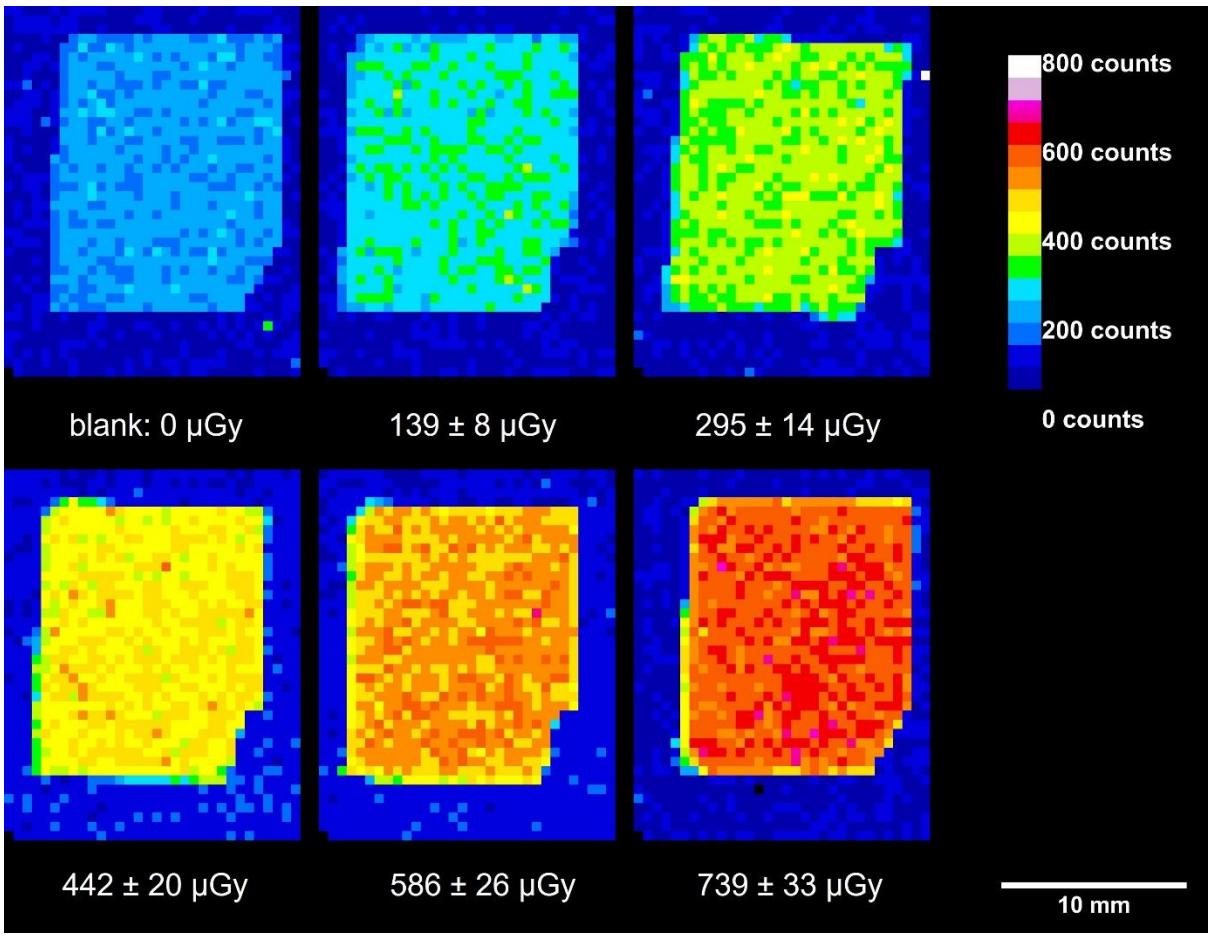

Figure 9 (1.5 column): OSL signal of piece of Al_2O_3:C film irradiated by a ^{60}Co gamma source. *The uncertainties on the gamma dose are provided at the 95% confidence level. The uncertainties on the average counts per pixel are negligible.*

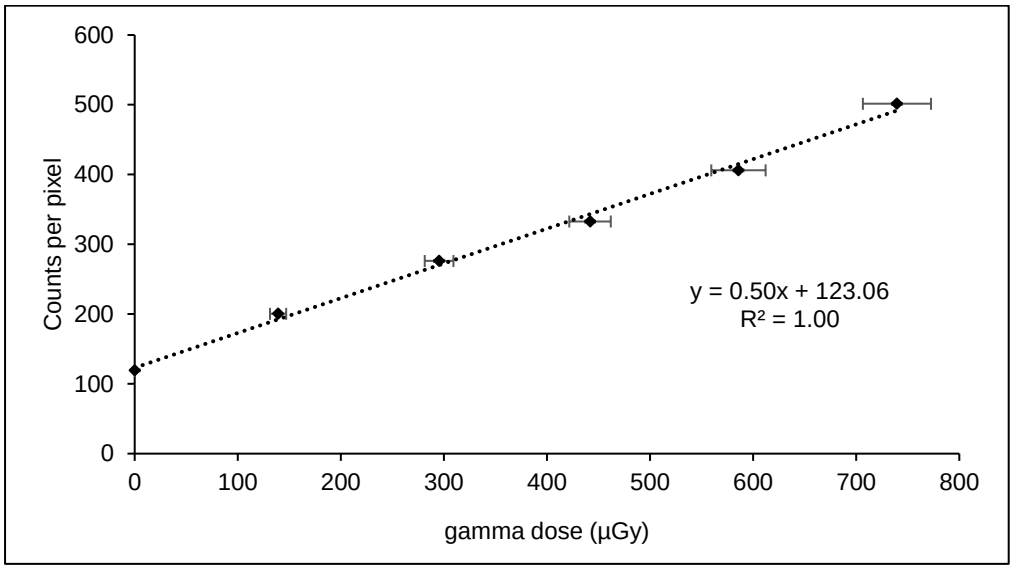

Figure 10 (single column): Detection and quantification limits for a piece of Al_2O_3:C film

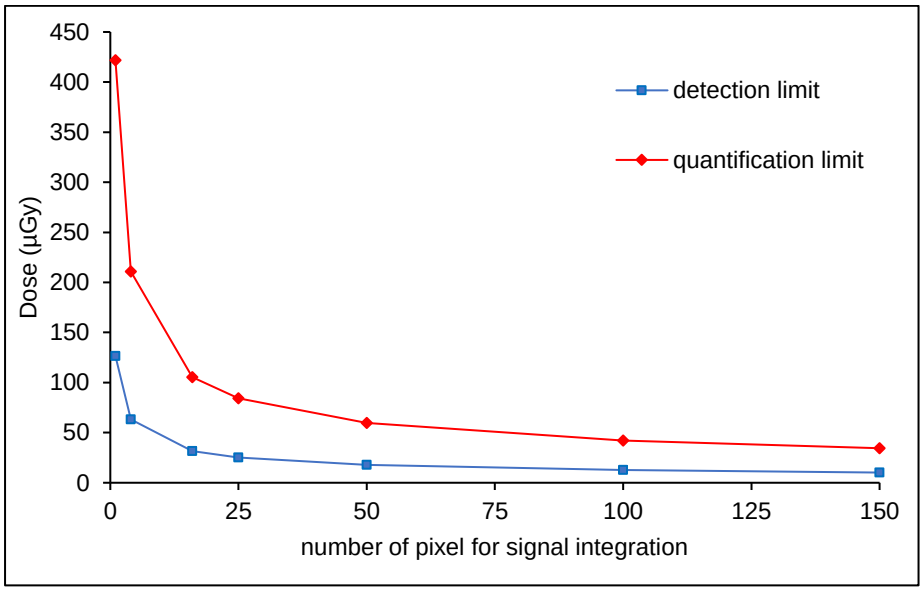

Figure 11 (1.5 column): Calibration curve and comparison of calculated dose with equivalent gamma dose. *The counts were averaged over the whole surface of the dose image recorded by the dosimeter except the edges, for a total of about 5500 pixels of 250 µm per image. The dark count and the phosphor background signal were subtracted from the results of graph a, so the remaining offset of 94* ± 31 cps *corresponds to the environmental background dose. This environmental background was additionally subtracted for graph b in order to highlight only the relation between calculated doses and equivalent gamma doses . The uncertainties on the calculated dose are provided at the 95% confidence level.*

a - OSL signal from exposure of dosimeter film pieces to powder samples. *The uncertainties on the average counts per pixel is inferior to 1%.*

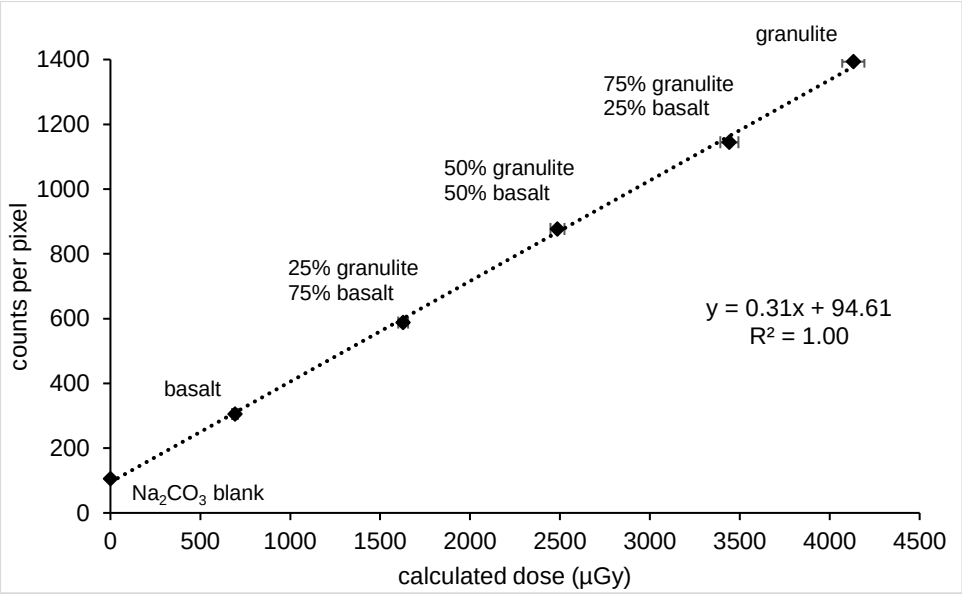

b – Comparison of the calculated dose for each sample exposure with the equivalent gamma dose. *The additional uncertainty on the normalized dose is due to the uncertainty on the gamma source dose rate (145 ± 7 µGy.h^{-1})*

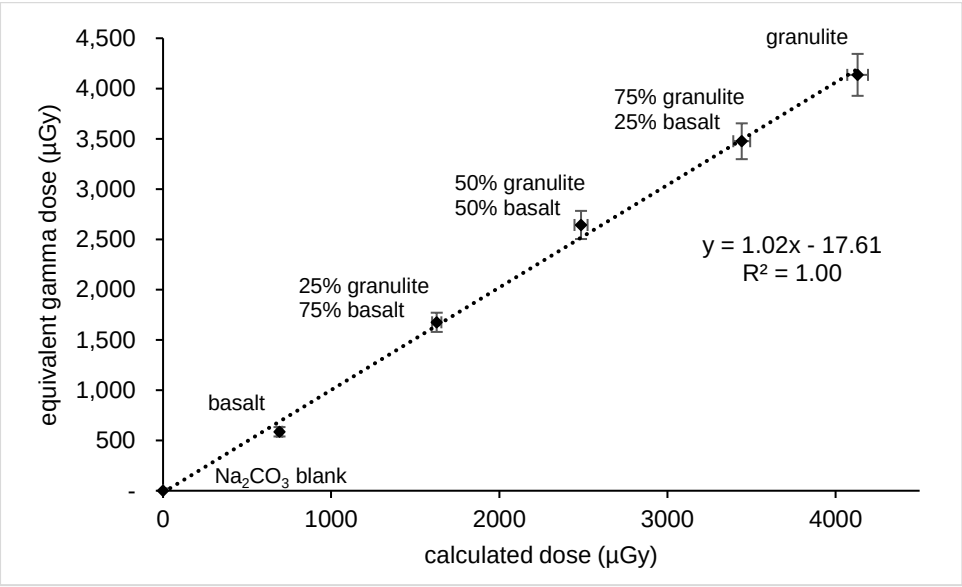

Figure 12 (1.5 column): beta dose profiles from Geant4 simulations

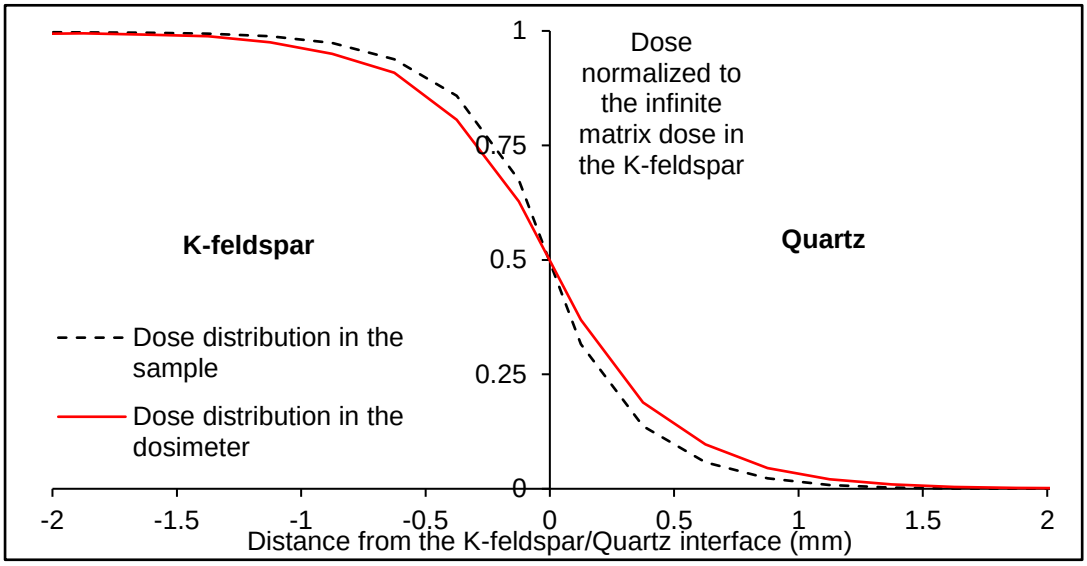

Figure 13 (single column): Environmental radiation shielding at the STFC Boulby Underground Laboratory

a – 5 cm thick copper brick shielding

b – Zeplin lead shield

Table 1 (single column): Radioactive element contents in the powder samples. *The uncertainties are provided at the 95% confidence level.*

Powder composition	K content (wt.%)	U content (ppm / $mg.kg^{-1}$)	Th content (ppm / $mg.kg^{-1}$)
Granulite 100%	3.46 ± 0.06	6.90 ± 0.12	16.9 ± 0.3
Granulite 75% - Basalt 25%	2.71 ± 0.05	5.50 ± 0.11	13.7 ± 0.2
Granulite 50% - Basalt 50%	1.96 ± 0.04	4.09 ± 0.10	10.5 ± 0.2
Granulite 25% - Basalt 75%	1.21 ± 0.03	2.69 ± 0.09	7.35 ± 0.2
Basalt 100%	0.46 ± 0.02	1.28 ±0.08	4.2 ± 0.1

Table 2 (single column): beta dose rate attenuation during dosimeter film exposure to powder samples. *These values were calculated by simulation. The uncertainties are provided at the 95% confidence level.*

spectra	Beta attenuation factor*	Gamma dose rate contribution*
^{40}K	0.680 ± 0.002	0.0402 ± 0.0006
U-series	0.638 ± 0.001	0.1447 ± 0.0004
Th-series	0.581 ± 0.001	0.1169 ± 0.0004
Granulite **	0.66 ± 0.01	0.101 ± 0.001
Basalt **	0.65 ± 0.01	0.169 ± 0.002
Typical sediment ***	0.65 ± 0.01	0.128 ± 0.001

** Given as ratio of the corresponding infinite matrix dose rate of the sample*

*** See table 1 for radioactive element contents*

**** ^{40}K 1 %, U 3 ppm, Th 10 ppm (Aitken, 1985)*